Real-Time Disturbance Detection in LV Islanded Microgrid

Anusuya Arunan, Jayashri Ravishankar and Eliathamby Ambikairajah
School of Electrical Engineering and Telecommunications, University of New South Wales, Sydney, Australia

***Abstract*— The rate of change of frequency following any disturbance in LV islanded microgrids is not only relatively high compared to conventional system, but also becomes location specific, due to their high R/X ratio lines. This makes the disturbance detection challenging. Conventional power imbalance calculation methods are not applicable due to variation of inertia with time. This paper proposes a novel real-time disturbance detection technique, independent to the system inertia. Three different Support Vector Machine regression models are created with three different feature selections. Results show that, some local parameters such as voltages at different locations should also be included with the frequency features for the accurate disturbance detection. This method can detect the amount of load disturbance within 0.5 second following the disturbance. The proposed algorithm is tested with an unseen test data. A multi-source islanded microgrid is used to collect the data, which is modelled in MATLAB/SIMULINK.**

***Index Terms*-- islanded microgrid, rate of change of frequency, real-time disturbance monitoring, feature extraction, support vector machine regression.**

I. Introduction

A microgrid is composed of distributed generations, loads, energy storage, secondary loads and controllers which cover the electrification of a small geographical area, and can be operated in grid connected mode as well as islanded mode [1]. Even though microgrids provide environmental friendly power supply through renewable sources, it creates stability, reliability and quality issues due to unpredictable renewable sources [2]. These issues are of more concern in islanded microgrids compared to grid connected microgrids because in grid connected mode, system parameters can be maintained by the conventional grid. In case of islanded operation, frequency, voltage and power balance should be handled by the microgrid itself. Higher dynamics and wider range of interactions between microgrid loads and small-scale generations may challenge the islanded microgrid operation. This results in more frequent and longer voltage and frequency variations[3]. As distributed generations in microgrid normally rely on inverter based renewable sources, they do not have enough kinetic energy. This decrease in kinetic reserve in renewable based islanded microgrids leads to stability issues [4].

When it comes to improving the stability limits for microgrids, traditional power system stabilizers and excitation systems are not applicable because of the lack of spinning reserve in microgrids [5]. Further, due to the low physical inertia of the microgrid, the dynamic response is much quicker than the conventional rotating machines, which makes the system potentially susceptible to oscillations, resulting from network disturbances[6],[7]. Thus, Rate of Change of Frequency(RoCoF) following any disturbance is relatively high compared to conventional systems.

RoCoF is proportional to the amount of disturbance in supply or demand and inversely proportional to the level of system inertia at the time of consideration. The greater the size of the disturbance event, or lower the system inertia, the faster the frequency will change. Thus, the level of system inertia in the islanded microgrid determines the size of the immediate RoCoF that would result following any disturbance. Further, the rate at which system frequency changes determines the amount of time that is available to arrest any drop or increase in frequency before it moves outside of the permitted operating frequency bounds. Therefore, the system should have the capability to detect the disturbance in detail within a short period of time [8],[9]. This is very important to perform any load shedding that may be required to correct the power imbalance.

Existing literature regarding power imbalance calculation for load shedding mostly follow the conventional methods [10]. But, traditional load shedding methods of conventional systems are not applicable for microgrids because of low inertia and mechanical power variation of energy sources with time. A multi stage under frequency load shedding algorithm has been proposed to calculate the power deficit in [11]. However, it is not descriptive in terms of where to shed load and when to shed load. Ajit A. Renjit et al. [12] presented a novel method to identify the power deficit in an islanded microgrid by using RoCoF and frequency nadir (the minimum value of frequency) of frequency oscillation. It was shown that the reduced order state space model performs well to calculate the power deficit of an islanded microgrid following any disturbance. Even though the variation of mechanical power had been considered in their work, the equivalent inertia of the system is fixed at a constant value all the times. An adaptive load shedding scheme in [13] and multistage under frequency load shedding in [14] were based on conventional methods. In these, theoretical deviations of microgrids from conventional systems were not

978-1-5386-0517-2/18/$31.00 ©2018 IEEE

considered well. Most of the conventional load shedding schemes are implemented with the only consideration of RoCoF. But this is not enough for islanded microgrids, as it is very sensitive to minor changes. Therefore, a fast and reliable method, independent to the microgrid parameters, like system inertia, would be a better solution for islanded microgrids.

In addition to the above limitations in the current literature, the system wide RoCoF was taken to apply in the power system swing equation for the power deficit calculation. In this paper, it is shown that the RoCoF will vary at different disturbance points due to high R/X ratio lines in islanded microgrids, even though the system frequency is unique. For example, the same amount of disturbance at different locations will create different RoCoF values. It depends on the distance of the disturbed location from the swing generation. This paper presents an in-depth analysis on this issue and by overcoming all the limitations identified above, it proposes a novel method to detect the amount of load disturbance in real-time for LV islanded microgrids. To achieve this, in addition to the system wide frequency measurement, local voltages at each load bus are also measured. As a small scale islanded microgrid has limited number of generation busses and load busses, it is possible to collect voltage data at all the busses by using the new sensors with high sampling rate and GPS technology as explained in CIGRE/CIRED JWG C4.24[3] .

The proposed method, in this paper, has the capability to detect the disturbance details in 0.5second, immediately after the occurrence of the disturbance. This method does not rely on system inertia. Support vector machine regression is used to detect the amount of disturbance with an appropriate feature selection. A multi-source islanded microgrid with energy storage and five load feeders with distribution lines as shown in Figure. 1 is modelled in MATLAB/SIMULINK to perform this analysis.

Architecture and functionality of the multi-source islanded microgrid is given in section II. Data collection procedure is explained in section III. Disturbance detection algorithms along with feature extraction technique for three different cases are shown in section IV. The proposed method has been applied to this multi-source microgrid system and the results are discussed in section V. Conclusions are outlined in Section VI.

II. Islanded Microgrid Model

A multi-source islanded microgrid, including wind power, solar power and synchronous generator along with battery storage system and five load banks with distribution lines is modelled in MATLAB/SIMULINK. It is 50Hz, 480V line to line voltage, three phase balanced system. Overall architecture of the islanded microgrid is shown in Figure 1.

A. Synchronous Generator

A 3-phase synchronous machine is modelled in the dq reference frame. This is the swing generation in the system, rated to 300kVA. Synchronous voltage regulator combined with an excitation system is implemented in this model [15]. The governor and exciter are controlling the current of the rotor field winding, which directly affects the terminal voltage of the generator [16]. Synchronization of the diesel generator to the

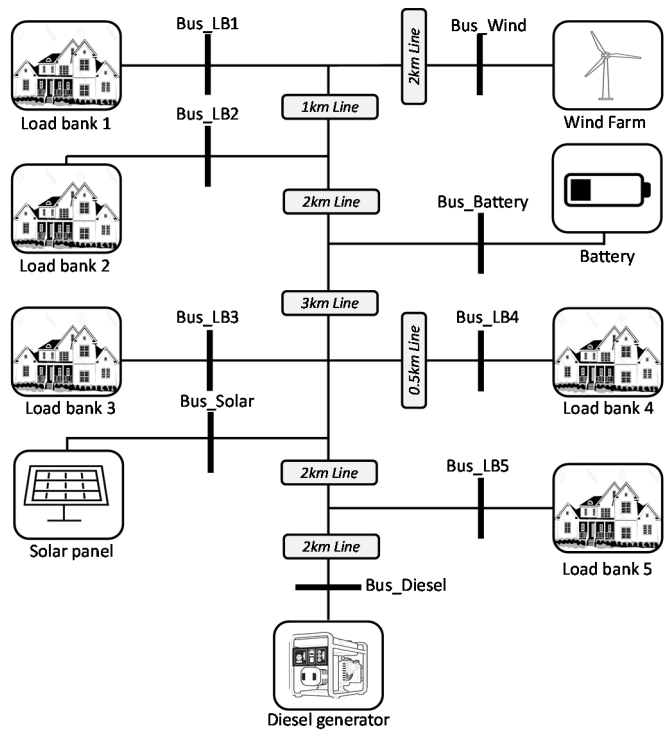

Figure 1. Microgrid architecture

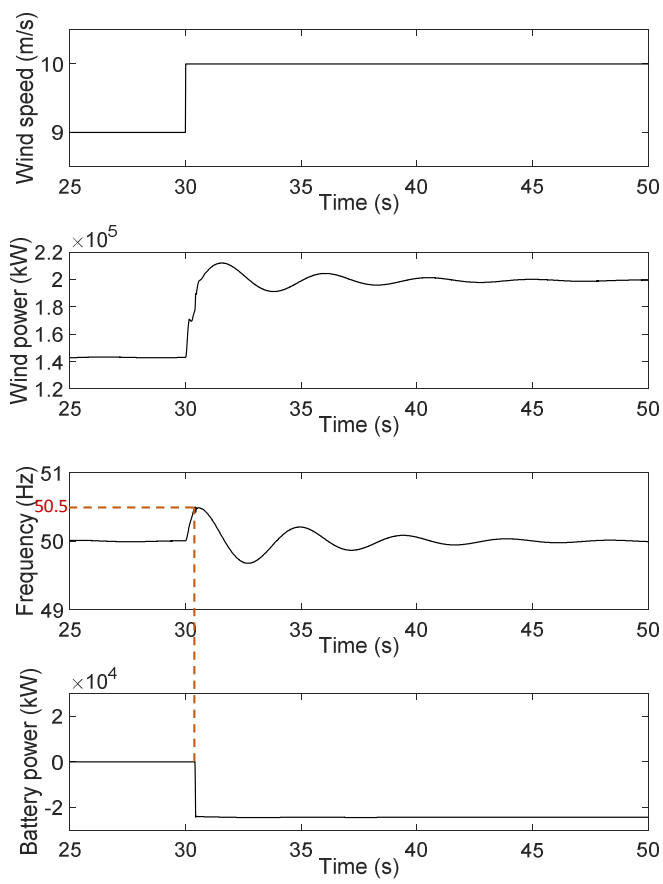

Figure 2. Variation of wind power output with varying wind speed

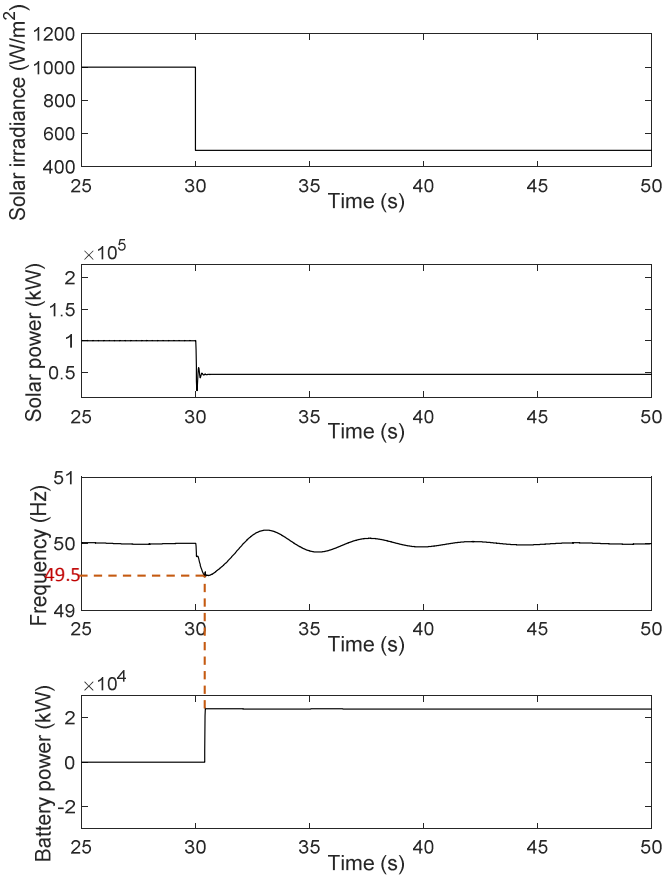

Figure 3. Variation of solar power output with varying solar irradiance

distribution network is done by matching the voltage, phase and frequency.

B. Wind Power Generation

The standard squirrel cage asynchronous machine of rating 275 kVA is modelled as wind turbine. The wind turbine has the option to change the wind speed. Figure 2 shows that as the wind speed increases, the wind power output also increases.

C. Solar Power Generation

The standard average inverter model has been used in this simulation with Maximum Power Point Tracking (MPPT). A single diode PV cell model was developed with the capability to vary output power depending on irradiance level as shown in Figure 3. It can be observed that as solar irradiance increases, output power from the PV inverter also increases in step. An average VSC model was used and this model does not require PWM switching, instead it uses the reference voltage waveforms. The PV source is set to deliver 100kW at 1000W/m^2 irradiance.

D. Energy Storage System

Energy storage system includes a battery model with inverter. It is a 100Ah, lead acid battery with 500V nominal voltage. It can be operated as charging, discharging and standalone mode. A control mechanism to change the mode of battery operation has been provided. During the steady state operation of the microgrid, battery will be in standalone mode. If the frequency of the microgrid goes below 49.5Hz, battery will change to discharging mode and it will supply extra power to the network and if the frequency goes above 50.5Hz battery will change to charging mode and it will consume the power from the network. These can be observed in Figure 2 and Figure 3.

E. Load and Distribution Lines

All the load banks are three phase, balanced, constant power, linear loads with the base power of each load bank being 140kW, 120kW, 140kW, 90kW and 95kW in load bank 1, load bank 2, load bank 3, load bank 4 and load bank 5 respectively. The total length of the distribution line is 12.5km with highly resistive and negligible inductive line parameters.

III. Data Collection

Two different steady state conditions have been obtained with different wind speeds, **State 1:** with 9m/s and **State 2:** with 10m/s, with constant solar irradiance level of 1000W/m^2 in both states. In each steady state operation, various load disturbances are created and the system frequency and per unit (pu) rms voltages at each load bank bus have been collected for each disturbance. The sampling frequency for the measurement used here is 20 kHz. Load disturbances are created at 25th second as

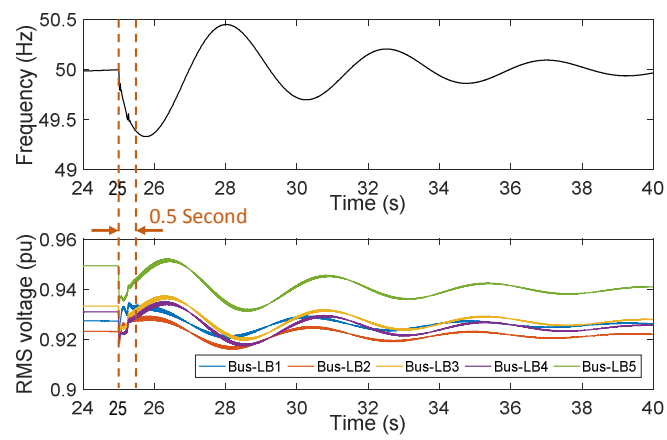

Figure 4. Frequency and voltage oscillation for disturbance

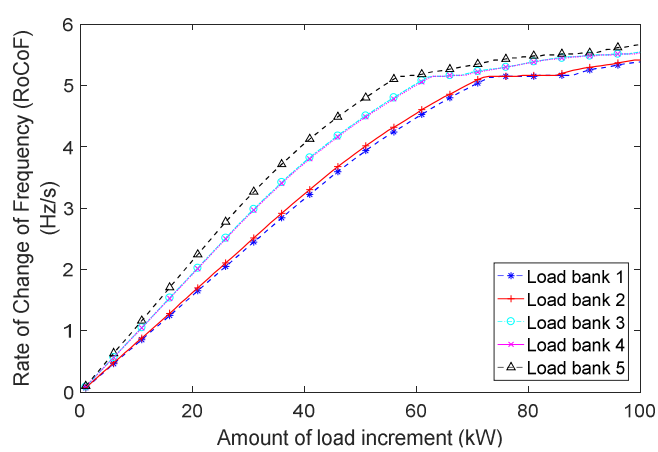

Figure 5. Rate of change of frequency with amount of load increment at each load bank

shown in Figure 4 in a wide range, up to 100kW load increment from base load in steps of 1kW at each load bank. While disturbing one load bank, all the other load banks are kept at their base load values. This is repeated to both steady state operations. In this manner, altogether 500 load disturbance data are collected one by one in each steady state operation.

RoCoF versus amount of load increment for each load bank is plotted at the steady state operation with the 10m/s wind speed and 1000W/m^2 (state 2), shown in Figure 5. It can be clearly seen that the RoCoF for the same amount of load increment is different for each load bank. RoCoF for the same amount of load increment is decreasing with the distance to the disturbance point from the swing generation. Since the distance to load bank 3 and load bank 4 from the swing generation is nearly the same, their RoCoF values are approximately coinciding.

IV. Disturbance Detection Algorithm

A. Feature Extraction

As the dynamic response is much quicker in islanded microgrids [6], 0.5 second data immediately after the disturbance is used for the analysis as shown in Figure 4. Figure 6 shows the block diagram of the feature extraction process.

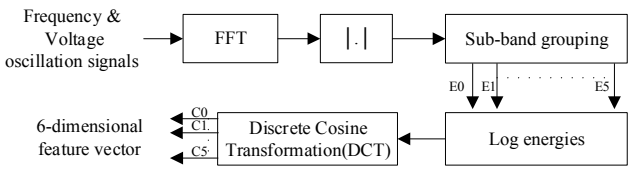

Figure 6. Feature extraction process

The Fast Fourier Transform (FFT) of the 0.5 second signal, sampled at 20kHz, is obtained and the magnitude of FFT is retained. FFT bins are grouped into 11octave sub-bands(SB) as shown in Figure 7. Since voltage and the frequency signal have very low frequency components [17], first 6 band energies are considered in this experiment, and average energies (E0, E1……. E5) corresponding to each sub-band are calculated. The log energies are smoothed using Discrete Cosine Transformation (DCT). In addition, the RoCoF value of the frequency oscillation immediately after the disturbance is also taken into consideration. Thus, altogether 37-dimensional feature vector is obtained (see Figure 8) from each disturbance data including RoCoF and 6 sub-band energy based features (system frequency and 5 load bank bus voltages).

B. Case Studies

Calculation of the amount of disturbance has been considered as a regression problem. Support Vector Machine Regression (SVR) is used to identify the amount of disturbance. Three different cases are considered for regression modeling by selecting different set of features as below.

Case 1: Only the RoCoF is considered as the feature for regression (1-dimensional feature vector, the first feature in Figure 8).

Case 2: Sub-band energy based features of frequency signal are also considered with RoCoF (7-dimensional feature vector, First 7 features in Figure 8).

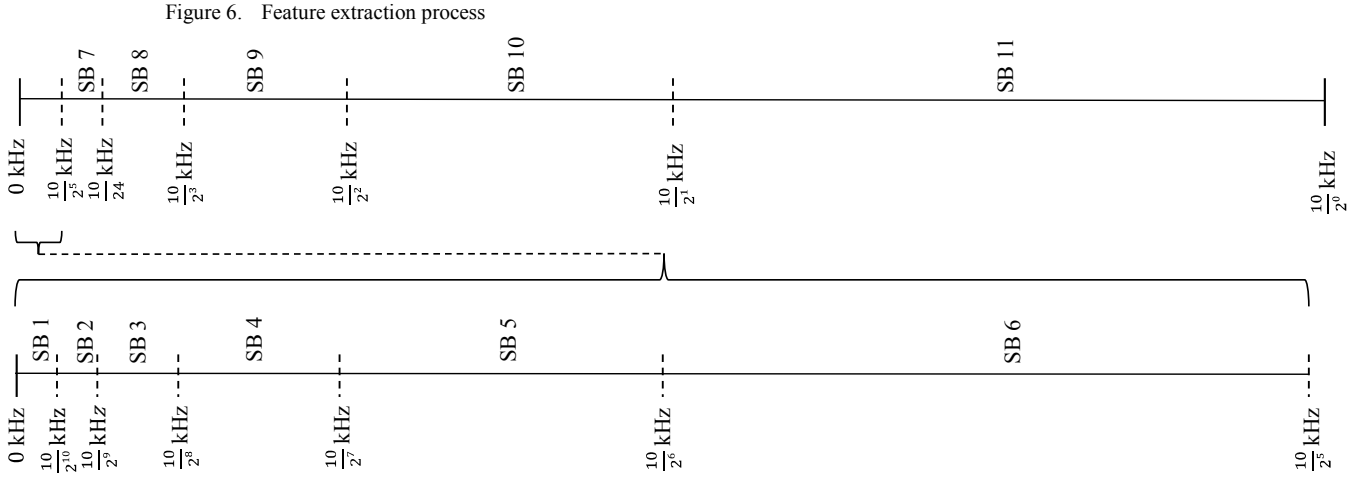

Figure 7. Octave sub-band divisions

1	2-7	8-13	14-19	20-25	26-31	32-37
RoCoF	Energy features from Microgrid frequency	Energy features from Voltage at Bus_LB1	Energy features from Voltage at Bus_LB2	Energy features from Voltage at Bus_LB3	Energy features from Voltage at Bus_LB4	Energy features from Voltage at Bus_LB5

Figure 8. Feature vector arrangement

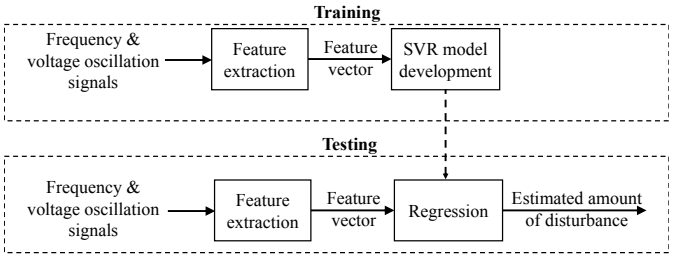

Figure 9. Proposed algorithm

Case 3: Sub-band energy based features of all load band voltages are also considered in addition to the case 2 features (37-dimensional feature vector, all 37 features in Figure 8).

In all three cases, for training, the state 1 data set is used, and the state 2 data set is unseen in the training phase. Then the state 2 data set is used for testing. The overall structure of the algorithm is shown in figure 9.

V. Results and Discussion

Lower the Mean Squared Error (MSE) of a regression model is better in performance. MSE for the unseen test data set (state 2) of the above three cases are compared. As shown in Table I, where 37-dimensional vector (Case 3) provides better results compared to other two cases.

TABLE I. Mean Squared Error For Each Case

Case No	Mean Squared Error (MSE)/kW^2
Case 1	35.0743
Case 2	15.7984
Case 3	1.93564

Further, individual error magnitudes for each unseen test data is calculated as below,

|Error|=|Actual amount of disturbance – estimated amount of disturbance through regression|

For an example, error magnitudes for the unseen test data of disturbance at load bank 5 is shown in Figure 10. It can be clearly seen that case 1 has higher value of errors, compared to other two cases, going up to 15kW. For case 3 the error values are quite low, less than 2kW. Therefore, case 3 is performing well compared to other two cases. By considering the above results, it can be clearly said that, even though the RoCoF is the only parameter in conventional systems for disturbance amount calculation, the small-scale LV islanded microgrid with high R/X ratio, relies on some other local parameters as well for more accurate disturbance amount calculation.

Same amount of disturbance at different location creates slightly different RoCoF values in a LV islanded microgrid due to highly resistive distribution lines. In summary, only the RoCoF or some other features of the system wide frequency measurement is not sufficient for the disturbance amount detection for a small-scale LV islanded microgrid. Other

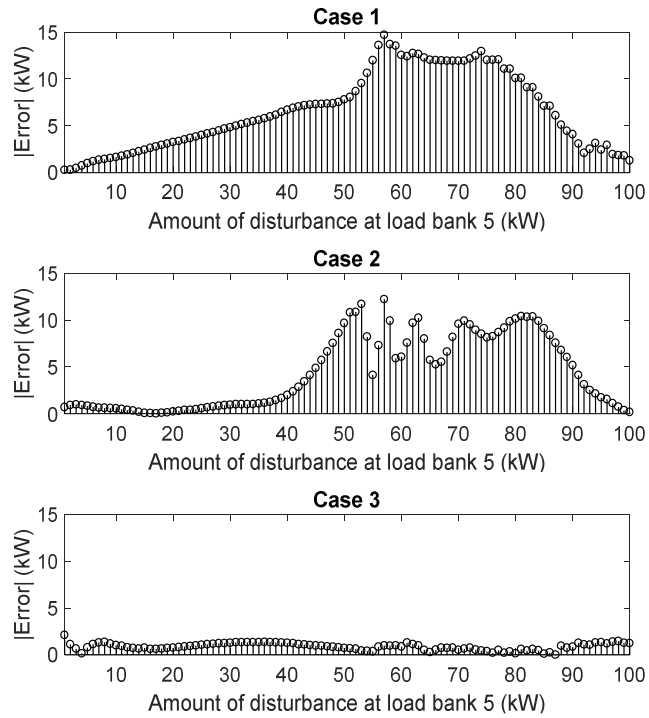

Figure 10. Regression error with amount of disturbance for all three cases in load bank 5

location specific parameters like voltage measurement at different locations also need to be taken into consideration for better disturbance detection.

VI. Conclusion

Low mechanical inertia and less kinetic reserve in inverter based islanded microgrids leads to high RoCoF values following any disturbance. Thus, less time is available compared to conventional systems, to arrest the system frequency before reaching the standard limits. Therefore, system should have the capability to detect the disturbance within a short period of time following the disturbance. However, the conventional power deficit calculation methods are not applicable due to mechanical power variation with time. Additionally, RoCoF is location specific in LV islanded microgrids due to high R/X ratio. Disturbance near to swing generation creates higher RoCoF compared to the disturbances far away from the swing generation.

In this paper, it is shown that the RoCoF value for the same amount of disturbance will vary depending on disturbance locations, due to high R/X ratio distribution lines in LV islanded microgrids, even though the system frequency is unique. Further, a novel real-time load disturbance amount detection algorithm is introduced. It is not only independent to the mechanical power variation of the system but also capable to detect the disturbance within 0.5 second following the disturbance. The algorithm includes octave band FFT energy based features of both frequency and local voltage measurements, in addition to RoCoF. This method can be extended to other real-time disturbance monitoring including detection of location of disturbance and type of disturbance, for a multi-source LV islanded microgrid. Such disturbance

detection methods, would help perform real-time stability analysis and enhancement for LV islanded microgrids, as they are dominant with real-time random factors.

VII. References

[1] L. Mariam, M. Basu, and M. F. Conlon, "Microgrid: Architecture, policy and future trends," *Renewable and Sustainable Energy Reviews*, vol. 64. pp. 477–489, 2016.

[2] K. P. Detroja, "Optimal autonomous microgrid operation: A holistic view," *Appl. Energy*, vol. 173, pp. 320–330, 2016.

[3] F. Zavoda *et al.*, "Power quality in the future grid - Results from CIGRE/CIRED JWG C4.24," *Proc. Int. Conf. Harmon. Qual. Power, ICHQP*, vol. 2016–Decem, pp. 931–936, 2016.

[4] M. Farrokhabadi, C. A. Cañizares, and K. Bhattacharya, "Frequency control in isolated/islanded microgrids through voltage regulation," *IEEE Trans. Smart Grid*, vol. 8, no. 3, pp. 1185–1194, 2017.

[5] A. M. Bouzid, J. M. Guerrero, A. Cheriti, M. Bouhamida, P. Sicard, and M. Benghanem, "A survey on control of electric power distributed generation systems for microgrid applications," *Renew. Sustain. Energy Rev.*, vol. 44, pp. 751–766, 2015.

[6] Z. D. Arani, S. A. Taher, A. Ghasemi, and M. Shahidehpour, "Application of Multi-Resonator Notch Frequency Control for Tracking the Frequency in Low Inertia Microgrids Under Distorted Grid Conditions," *IEEE Trans. Smart Grid*, vol. 3053, no. c, pp. 1–12, 2017.

[7] M. Brenna, G. C. Lazaroiu, G. Superti-Furga, and E. Tironi, "Bidirectional front end converter for DG with disturbance insensitivity and islanding-detection capability," *IEEE Trans. Power Deliv.*, vol. 23, no. 2, pp. 907–914, 2008.

[8] N. Golovanov, G. C. Lazaroiu, M. Roscia, and D. Zaninelli, "Power quality assessment in small scale renewable energy sources supplying distribution systems," *Energies*, vol. 6, no. 2, pp. 634–645, 2013.

[9] R. Pourramezan, Y. Seyedi, H. Karimi, G. Zhu, and M. Mont-Briant, "Design of an Advanced Phasor Data Concentrator for Monitoring of Distributed Energy Resources in Smart Microgrids," *IEEE Trans. Ind. Informatics*, pp. 1–1, 2017.

[10] N. N. A. Bakar, M. Y. Hassan, M. F. Sulaima, M. N. im Mohd Nasir, and A. Khamis, "Microgrid and load shedding scheme during islanded mode: A review," *Renew. Sustain. Energy Rev.*, vol. 71, no. November 2016, pp. 161–169, 2017.

[11] A. Ketabi and M. H. Fini, "Electrical Power and Energy Systems An underfrequency load shedding scheme for islanded microgrids," *Electr. Power Energy Syst.*, vol. 62, pp. 599–607, 2014.

[12] A. A. Renjit, A. Mondal, M. S. Illindala, and A. S. Khalsa, "Analytical Methods for Characterizing Frequency Dynamics in Islanded Microgrids with Gensets and Energy Storage," in *IEEE Transactions on Industry Applications*, 2017, vol. 53, no. 3, pp. 1815–1823.

[13] M. Marzband, M. Mirhosseini, and M. Funsho, "Adaptive load shedding scheme for frequency stability enhancement in microgrids," *Electr. Power Syst. Res.*, vol. 140, pp. 78–86, 2016.

[14] W. Gu, W. Liu, C. Shen, and Z. Wu, "Multi-stage underfrequency load shedding for islanded microgrid with equivalent inertia constant analysis," *Int. J. Electr. Power Energy Syst.*, vol. 46, no. 1, pp. 36–39, 2013.

[15] MathWorks, "Emergency Diesel-Generator and Asynchronous Motor," 2017.

[16] P. Singh, "Real time modeling and simulation of distribution feeder and distributed resourses," Dept. Electric. and Com. Eng, Colorada State University, 2015.

[17] S. A. Hosseini, N. Amjady, and M. H. Velayati, "A Fourier Based Wavelet Approach Using Heisenberg ' s Uncertainty Principle and Shannon ' s Entropy Criterion to Monitor Power System Small Signal Oscillations," *IEEE Trans. Power Syst.*, vol. 30, no. 6, pp. 3314–3326, 2015.